Near-field BER and EVM Measurement at 5.8 GHz in Mode-stirred Metal Enclosure

Mir Lodro, Chris Smart, Gabriele Gradoni, Ana Vukovic
Dave Thomas, and Steve Greedy

George Green Institute for Electromagnetics Research-GGIEMR
University of Nottingham, University Park, NG72RD, United Kingdom
mir.lodro@nottingham.ac.uk

Abstract – This work presents over-the-air (OTA) performance, near-field bit-error-ratio (BER), and error vector magnitude (EVM) measurement using software-defined radio (SDR) in the mode-stirred metal enclosure at 5.8 GHz. The metal enclosure is stirred at 5.8 GHz using metallic paddle rotating with uniform speed. Paddle rotation creates a uniform electromagnetic field in the metal enclosure. The electromagnetic field environment in the metal enclosure can be controlled by loading the cavity with absorbing material. Field absorption can be different depending on the amount of absorbing material and location of the absorbers in the metal enclosure. It is shown that signal attenuation increases as we increase the number of absorbers. BER and EVM are measured in this environment and the performance of SDR based digital receiver is analyzed in this environment at RF frequency of 5.8 GHz.

Index Terms – BER, EVM, Metal Enclosure, OTA Measurements, Reverberation Chamber, SDR, USRP B210.

I. INTRODUCTION

The metal enclosure is a perfectly reflecting environment and when stirred with mode-stirrer it acts as a small reverberation chamber (RC). This environment exhibits a rich isotropic multipath fading environment. It's suitable for testing for wireless communication systems. Reverberation chambers of various sizes have been traditionally used for electromagnetic compatibility and electromagnetic interference analysis, however, it has also been used for the testing of wireless communication system [1]. One or two mode-stirrers have been used to create multipath fading. With adequate stirring and the number of absorbers multipath fading can be controlled inside the chamber [2]. Reverberation chambers are also used for testing of antennas for determining the total radiation efficiency [3], radiated power [4], antenna efficiency [3, 5], backscattering measurement [6], diversity gain [7] and total isotropic sensitivity measurement [8]. BER measurements are performed in the reverberation chamber in [1]. Different techniques to create a specific multipath fading environment are present in the literature. SDR based measurements and SDR based testing of antennas are presented in [9] and [10, 11] respectively. RC has been used to test more sophisticated communication systems for throughput measurements [12]. We tested QPSK receiver in an anechoic chamber with USRP X310 and measured BER and OTA performance under different noise levels [13, 14]. This article is divided into five sections. After the introduction in Section I, Section II highlights the importance of near-field measurements, Section III explains transmitter and receiver baseband models. Section IV details the near-field measurement setup in the mode-stirred cavity. Section V shows measurement results. Section VI presents the conclusion and future aspect of this work.

II. NEAR-FIELD MEASUREMENTS

Near-field measurements are becoming popular as the generated traffic volume and the demand for high data rate transmission has grown manifolds. This has led to the quest for the design, development, and integration of high data rate short-range wireless communication in the near-field. The potential applications are in 5G/6G dense connectivity [15–17], server racks and wireless chip-to-chip communication or board-to-board communication [18]. The existing form of near-field communication takes place using inductive and capacitive coupling for contactless payment and short-distance smart readers for low-rate applications. However, it's not a feasible solution for applications that are area-constraint and require high transmission rates such as wireless inter-core communication and wireless chip-to-chip communication [19]. RF communica-

Submitted On: April 10, 2020
Accepted On: May 26, 2020

https://doi.org/10.47037/2020.ACES.J.350915

1054-4887 © ACES

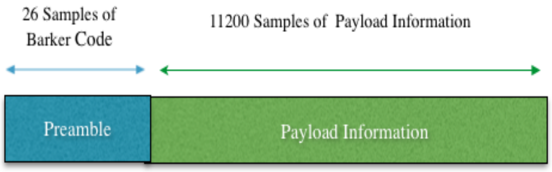

Fig. 1. Frame format of QPSK receiver.

tion using monopoles or printed patch antennas is required. Radiation boundary around antennas is classified in three regions as reactive near-field, radiative near-field, and far-field [20]. These fields are proportional to antenna dimension D and the operating wavelength of λ. Hence the reactive near-field:

$$Near-field = 0.62\sqrt{\frac{D^3}{\lambda}}. \tag{1}$$

For antenna dimension, $D = 8cm$, the near-field boundary in our case starts at $6cm$. However, the distance d between transmit and receive monopoles is around $5cm$ which is below the near-field boundary of $6cm$.

III. TRANSMITTER AND RECEIVER BASEBAND MODEL

A. Transmitter baseband model

QPSK transmitter consists of bits generation, QPSK modulation, and root raised cosine transmitter filter. Bits generation block generates frames of sample size 11226 × 1. Each frame consists on payload and preamble as shown in Fig. 1. The payload is useful data which is 100 ‘Hello World’ messages. The payload is scrambled to create an equal number of ones and zeros. Scrambling is helpful for timing recovery at the receiver. The preamble is created by using a 13-bit Barker code, and it is oversampled by a factor of two. Barker code exhibits excellent correlation properties, hence it’s suitable for frame detection. Scrambled bits produced by bits generation block are QPSK modulated. The modulated symbols are upsampled by raised cosine transmit filter with pulse shaping factor of 0.35. Raised cosine transmit filter produces samples at the rate of 400 kbps. These samples are transferred to B210 USRP from host PC over USB3.0 cable and after RF upconversion, signals are transmitted over the air.

B. Receiver baseband model

The receiver design is more challenging than the transmitter since multipath fading introduces signal attenuation, phase-shift, and delay in the transmitted signal. The received signal is not only affected by fading in the channel but other hardware imperfections at the transmitter and receiver including power amplifier non-linearity and filtering-imperfections. This signifies the complexity of wireless communication receiver design. Hence, the QPSK receiver consists of automatic gain control (AGC) which stabilizes weak signal amplitude as it’s important for optimum loop design for carrier symbol synchronization. AGC stabilizes the input signal to a constant level for subsequent stages in the QPSK receiver. Raised cosine receive filter performs matched filtering with the pulse-shaping factor of 0.35. Synchronization is vital for the optimal performance of the wireless receiver. Frequency and timing synchronization can be performed by using external 10 MHz reference (REF) and 1 pulse-per-second (PPS) timing signal from Octoclock-G or it can be performed using digital receiver blocks in the baseband model at host PC. We used digital synchronization stages to compensate for any frequency and timing offset. Hence, the QPSK receiver employs different synchronization stages such as coarse frequency compensation, symbol synchronization, carrier synchronization, and frame synchronization followed by the data decoding stage. Synchronization techniques for digital receiver design are discussed in [21–24].

1. *Coarse Frequency Compensation*: This stage of the digital receiver produces a rough estimate of frequency offset. This works on averaging of the output of the correlation-based algorithm. There is still a residual frequency offset present. The performance and accuracy of this stage are affected by the maximum frequency offset. Following coarse frequency compensation timing recovery and fine frequency compensation is performed.

2. *Symbol Synchronization*: Symbol synchronization performs timing recovery based on Gardner’s time-invariant algorithm. Timing recovery is achieved using PLL which is defined by normalized loop bandwidth, damping factor, and detector gain. Critically damped PLL locks quickly to correct symbol timing and hence introduces little *timing jitter*.

3. *Fine Carrier Synchronization*: This stage compensates the residual frequency offset present in the signal that was not compensated by the coarse frequency compensation stage. This stage uses PLL which tracks the residual frequency offset and phase offset in the signal. The damping factor and normalized loop bandwidth are tunable. PLL is critically damped so that it quickly locks to the intended phase while introducing little ’phase noise’.

4. *Frame Detection and Frame Synchronization*: Frame boundary detection is performed by a 13-bit Barker code that was used as preamble in the transmitted frames. Frame detection and frame alignment are done using the Barker code autocorrelation peak. The threshold designed for peak detection is critical for this block.

5. *Data Decoding*: Here phase ambiguity resolution, QPSK demodulation and payload retrieval is preformed. Phase ambiguity subsystem rotates the received signal by estimated phase offset and correct data is demodulated. Payload information is descrambled and decoding bits are converted to 'Hello World' characters visualized on diagnostic visualizer.

IV. MEASUREMENT SETUP

We have used a brass metal enclosure with dimensions of $h \times \ell \times w$ of $45\,cm \times 37\,cm \times 55\,cm$. The brass metal enclosure has a mode-stirrer whose rotation is controlled using a battery-operated motor. The metal cavity is a perfectly reflecting environment and when excited at 5.8 GHz it produces rich isotropic multipath (RIMP) fading environment. The sole purpose is to create a multipath fading environment. The Tx and Rx monopoles are in line-of-sight of each other. QPSK modulated signals are transmitted using USRP B210 which is connected to host PC over a USB cable. For parameters under consideration, there were some instances of underflow and overflow during the measurements and execution of the baseband model. USRP B210 is a low-cost RF solution for testing of wireless communication systems algorithms and RF measurements. USRPB210 is based on analog Devices AD9361 RFIC. It can operate in full-duplex 2x2 multiple-input multiple-out (MIMO) up to 56 MHz single-channel bandwidth. Figure 2 shows a measurement setup where two Tx and Rx monopoles are installed in near-field facing down in the cavity when the lid of the metal cavity is closed. The measurement setup shows mode-stirrer inside the brass cavity which stirs the electromagnetic field.

V. MEASUREMENT RESULTS

In this section, we show different measurement results recorded during the operation of the baseband model. The first component of the baseband receiver model is AGC which stabilizes the received signal and it's controlled using PLL. Figure 3 shows input to AGC and the stabilized signal with PLL step size. It's shown that PLL locks quickly when step size is increased from 0.001 to 0.01. Additionally, there could be a frequency offset present between transmitter and receiver. In Fig. 4 top plot shows frequency offset and the bottom plot shows mean frequency offset estimated at the receiver. This frequency offset can be compensated separately using separate baseband Tx and Rx models and subsequently removed at the receiver. Subsequent stages of the receiver include symbol timing error. Figure 5 shows timing error at the receiver. It can be seen that the timing errors are dominant at the start of the receiver. There are no timing errors after the SDR system has stabilized. Similarly Fig. 6 shows timing error recovery which struggles when there is low Tx gain.

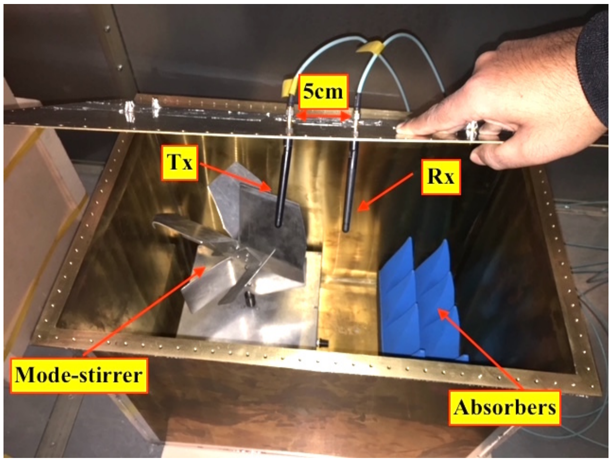

Fig. 2. SDR based near-field EVM and BER measurement setup in metal enclosure.

Table 1: System design parameters

Parameter	Values
Frequency	$5.8GHz$
Tx/Rx Antenna	Monopoles
Symbol Time	$5\mu s$
Sample Rate	$400KHz$
Payload Length	11200
Header Length	26
Message Bits	11200
Frame Time	$0.0281s$
Filter Order	10
Roll-off	0.35
USRP Frame Length	11226
USRP Interpolation Factor	50

Figure 7 shows detection metric for each received frame. This frame detection metric used to correctly decode the received frame if the metric exceeds a designed threshold. Figure 8 shows autocorrelation of full-frame which has a peak at 26th sample in the received frames which signifies the availability of Barker code based header of length 26.

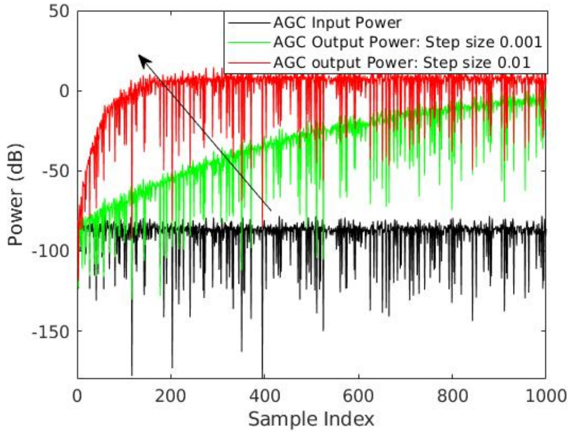

Fig. 3. Input and output of AGC with step size of 0.01 and 0.001 respectively.

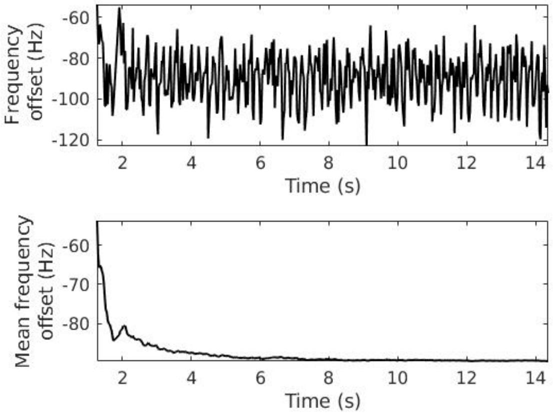

Fig. 4. Frequency offset and mean frequency offset estimation in (Hz).

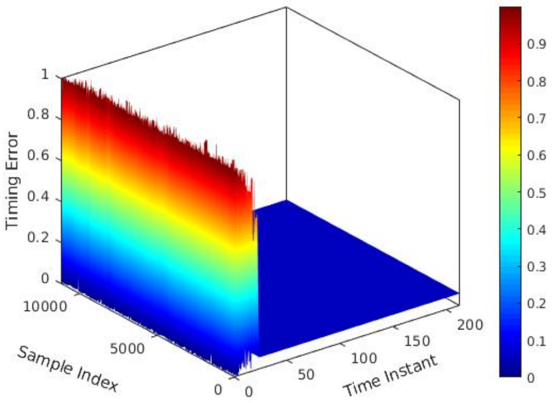

Fig. 5. Symbol timing error.

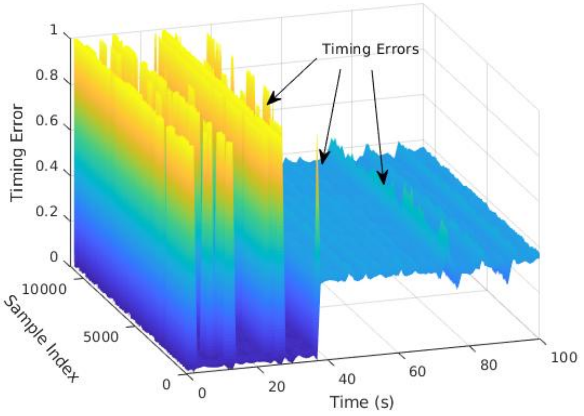

Fig. 6. Timing errors in the near-field at 5.8 GHz when Tx gain was 54 dB.

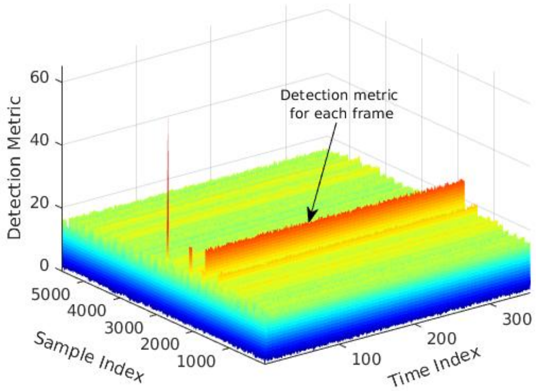

Fig. 7. Detection metric for each received frame.

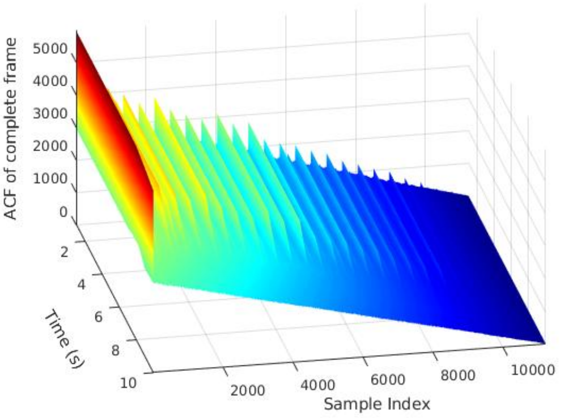

Fig. 8. Autocorrelation of full frame.

Figure 9 shows the diagram for the measurement of phase angle for phase ambiguity resolution. The output of the phase offset estimator subsystem that's used to correct phase ambiguity resolution of the QPSK system for data decoding is shown in Fig. 10.

Additionally, there were timing errors at low transmit gains and the QPSK constellation diagram converted into a blob of noise from ideal constella-

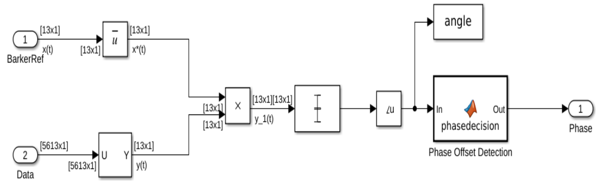

Fig. 9. Phase angle estimate block diagram.

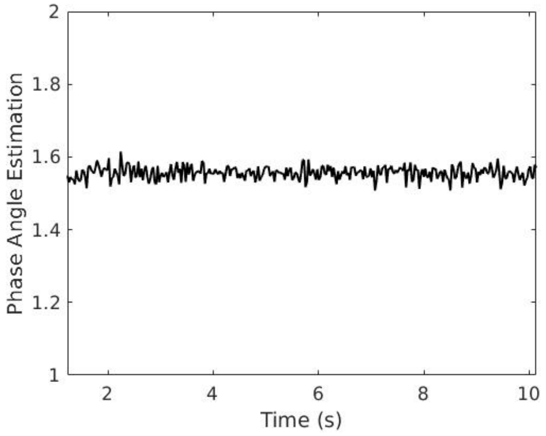

Fig. 10. Phase angle estimate for phase ambiguity resolution.

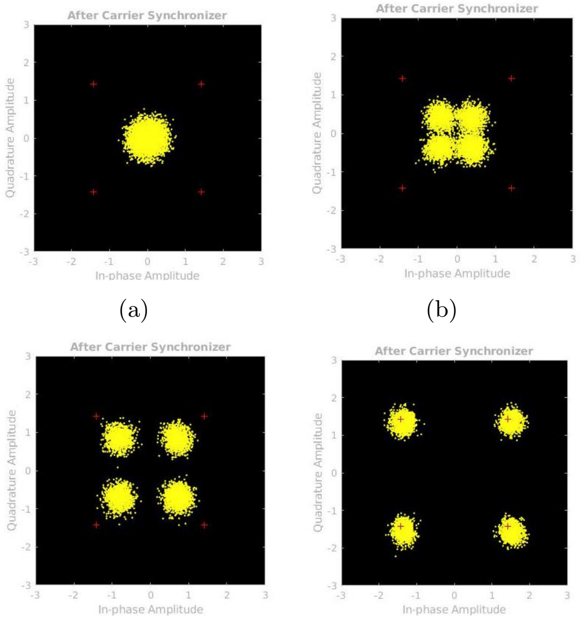

(a) (b)

(c) (d)

Fig. 11. QPSK constellation diagram at low Tx gains.

tion points and re-emerged smoothly to attain lock at ideal constellation diagram as shown in Fig. 11. The smashing and re-emergence of constellation diagram was continuously observed. This was consistent with the timing errors as shown in Fig. 5.

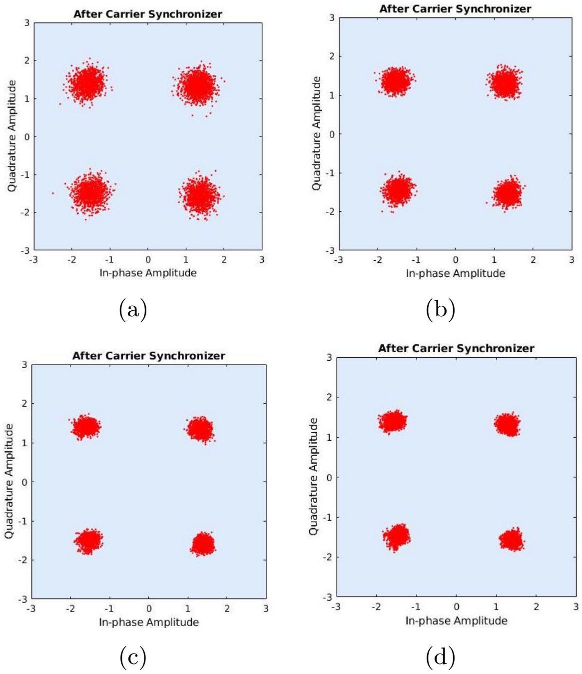

(a) (b)

(c) (d)

Fig. 12. QPSK constellation diagram after carrier synchronization: (a) Tx Gain=30 dB, EVM=16%, (b) Tx Gain=35 dB, EVM=12%, (c) Tx Gain=40 dB, EVM=11%, and (d) Tx Gain=45 dB, EVM=10%.

Figure 13 shows cross-correlation of 500 received packets with Barker code. A peak is observed at every 26th sample in the packet which is header length corresponds to 13-bit Barker code oversampled by a factor of 2.

A. EVM measurements

It's Euclidean distance between ideal constellation point and the received constellation points in IQ plane. Figure 12 shows a constellation diagram and corresponding measured EVM when the Tx gain was varied from 30 dB to 45 dB with a step size of 5 dB. With an increase in Tx gain hence an increase in SNR, the received QPSK samples get concentrated around ideal QPSK symbols. Such an increase in SNR also results in a decrease in EVM magnitude. It can be seen from Fig. 12 that EVM has decreased from 16% to 10%. Further increase in EVM is not observed in the current receiver structure because of the increased noise floor no matter how large we increase the gain. This behavior was observed in the far-field in large reverberation chamber under different fading conditions and indoor laboratory environments as well. Figure 14 shows instantaneous EVM in percent of QPSK at five runs. The EVM remains constant at around 11% EVM.

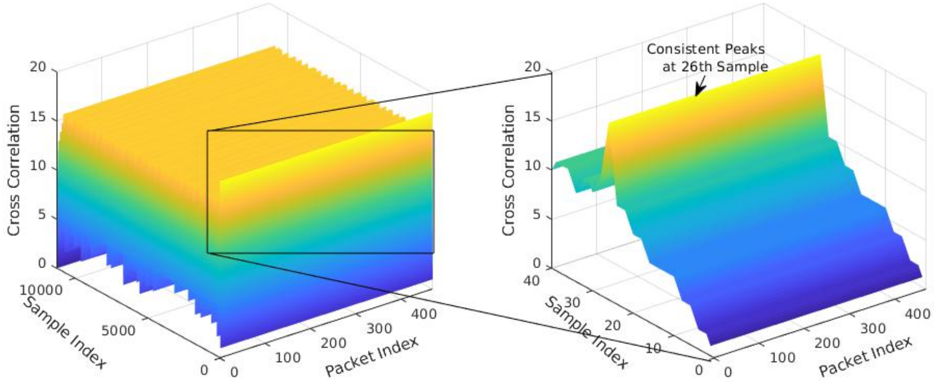

Fig. 13. Cross correlation of full frame and Barker code.

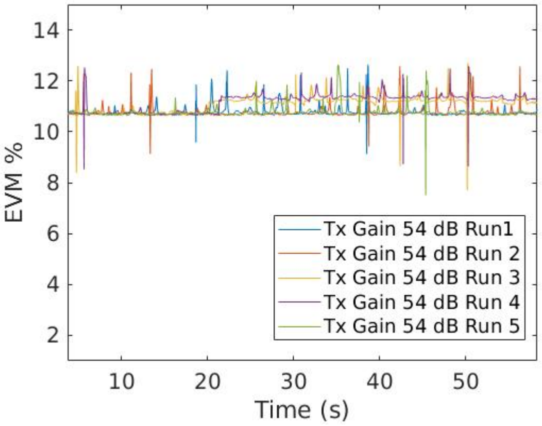

Fig. 14. EVM in the near-field at five runs when Tx gain is set to 54 dB.

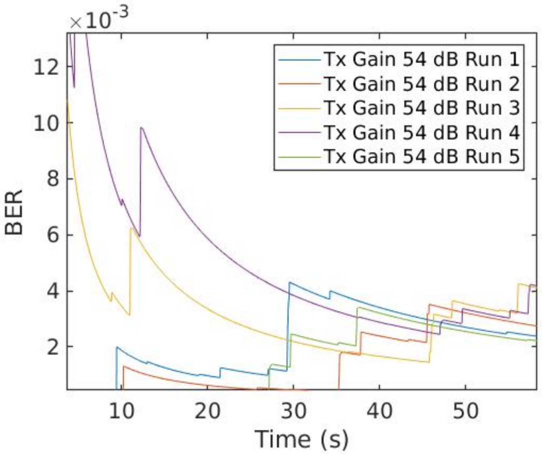

Fig. 15. BER measurements.

B. BER measurements

BER is one of the key performance indicators of digital communication systems, where the transmitted bits are compared with the received bits. If a large number of bits are erroneously received then the system has high BER, however, this is compensated by different receiver design stages as mentioned in previous sections. BER measurement is shown in Fig. 15. It can be seen that the BER at instants is very small and then there are transitions in BER curves. BER decreases at every run and it suddenly increases and then decreases. This is consistent with underflow and overflow in the system model. Underflow and overflow is an important issue for sensitive BER measurements using SDR. There could be other potential reasons to mention the degradation of BER. Shielding ineffectiveness of RF daughter boards in SDRs. The BER measurements are affected when the measurements are performed when Tx and Rx are located on the same RF cards. Variation in BER pattern can also be attributed to near-field effect or failure and instant recovery of one of the stages of the digital receiver including PLL based loops in carrier phase synchronization and timing recovery.

VI. CONCLUSION AND FUTURE WORK

In this work, we have shown the OTA performance of the digital receiver in near-field in a mode-stirred metal enclosure. The performance of different stages of the digital receiver is checked in the mode-stirred metal cavity. We measured AGC performance, frequency offset, timing error, and frame detection metrics of the digital receiver in the near-field. We observed that degradation factors of complete wireless communication system key performance indicators (KPIs) can be attributed to proper PLL design in the AGC, timing recovery, Tx/Rx gains, frame detection metrics. We performed BER measurement in the metal enclosure and enlisted possible BER degradation factors and suggested ways to overcome BER degradation factors. The future aspect of this study is to optimize BER and EVM measurements using meta-surface based Large Intelligent Surface (LIS) structures.

REFERENCES

[1] E. Genender, C. L. Holloway, K. A. Remley, J. M. Ladbury, G. Koepke, and H. Garbe, "Simulating the multipath channel with a reverberation chamber: Application to bit error rate measurements," *IEEE Transactions on Electromagnetic Compatibility*, vol. 52, no. 4, pp. 766–777, 2010.

[2] E. Genender, C. Holloway, K. Remley, J. Ladbury, G. Koepke, and H. Garbe, "Use of reverberation chamber to simulate the power delay profile of a wireless environment," in *2008 International Symposium on Electromagnetic Compatibility-EMC Europe*, pp. 1–6, IEEE, 2008.

[3] C. L. Holloway, H. A. Shah, R. J. Pirkl, W. F. Young, D. A. Hill, and J. Ladbury, "Reverberation chamber techniques for determining the radiation and total efficiency of antennas," *IEEE Transactions on Antennas and Propagation*, vol. 60, no. 4, pp. 1758–1770, 2012.

[4] G. Koepke and J. Ladbury, "Radiated power measurements in reverberation chambers," in *56th ARFTG Conference Digest*, vol. 38, pp. 1–7, IEEE, 2000.

[5] H. G. Krauthäuser and M. Herbrig, "Yet another antenna efficiency measurement method in reverberation chambers," in *2010 IEEE International Symposium on Electromagnetic Compatibility*, pp. 536–540, IEEE, 2010.

[6] A. Sorrentino, G. Ferrara, M. Migliaccio, and S. Cappa, "Measurements of backscattering from a dihedral corner in a reverberating chamber," *Newsletter-Applied Computational Electromanetic Society*, vol. 33, pp. 91–94, 2018.

[7] K. Rosengren and P.-S. Kildal, "Radiation efficiency, correlation, diversity gain and capacity of a six-monopole antenna array for a MIMO system: Theory, simulation and measurement in reverberation chamber," *IEE Proceedings-Microwaves, Antennas and Propagation*, vol. 152, no. 1, pp. 7–16, 2005.

[8] C. Orlenius, P.-S. Kildal, and G. Poilasne, "Measurements of total isotropic sensitivity and average fading sensitivity of CDMA phones in reverberation chamber," in *2005 IEEE Antennas and Propagation Society International Symposium*, vol. 1, pp. 409–412, IEEE, 2005.

[9] A. Hussain, B. P. Einarsson, and P.-S. Kildal, "Mimo ota testing of communication system using sdrs in reverberation chamber [measurements corner]," *IEEE Antennas and Propagation Magazine*, vol. 57, no. 2, pp. 44–53, 2015.

[10] A. Hussain, A. A. Glazunov, B. . Einarsson, and P.-S. Kildal, "Antenna measurements in reverberation chamber using USRP," *IEEE Transactions on Antennas and Propagation*, vol. 64, no. 3, pp. 1152–1157, 2016.

[11] P. Nayeri and R. L. Haupt, "A testbed for adaptive beamforming with software defined radio arrays," in *2016 IEEE/ACES International Conference on Wireless Information Technology and Systems (ICWITS) and Applied Computational Electromagnetics (ACES)*, pp. 1–2, IEEE, 2016.

[12] N. Olano, C. Orlenius, K. Ishimiya, and Z. Ying, "WLAN MIMO throughput test in reverberation chamber," in *2008 IEEE Antennas and Propagation Society International Symposium*, pp. 1–4, IEEE, 2008.

[13] M. Lodro, C. Smartt, I. Maricar, A. Vukovic, D. Thomas, and S. Greedy, "BER measurement and OTA performance of QPSK receiver in an anechoic chamber," 2018.

[14] M. Lodro, "BER measurements and RF performance of digital wireless communication systems using USRP X310," *Measurements*, p. 1/40, 2018.

[15] A. Costanzo and D. Masotti, "Energizing 5G: Near-and far-field wireless energy and data trantransfer as an enabling technology for the 5G IoT," *IEEE Microwave Magazine*, vol. 18, no. 3, pp. 125–136, 2017.

[16] Z. Zhang, Y. Xiao, Z. Ma, M. Xiao, Z. Ding, X. Lei, G. K. Karagiannidis, and P. Fan, "6G wireless networks: Vision, requirements, architecture, and key technologies," *IEEE Vehicular Technology Magazine*, vol. 14, no. 3, pp. 28–41, 2019.

[17] W. Saad, M. Bennis, and M. Chen, "A vision of 6G wireless systems: Applications, trends, technologies, and open research problems," *IEEE Network*, 2019.

[18] J. Karedal, A. P. Singh, F. Tufvesson, and A. F. Molisch, "Characterization of a computer board-to-board ultra-wideband channel," *IEEE Communications Letters*, vol. 11, no. 6, pp. 468–470, 2007.

[19] H. Yordanov and P. Russer, "Wireless inter-chip and intra-chip communication," in *2009 European Microwave Conference (EuMC)*, pp. 145–148, IEEE, 2009.

[20] C. A. Balanis, *Antenna Theory: Analysis and Design*, John Wiley & Sons, 2016.

[21] U. Mengali, *Synchronization Techniques for Digital Receivers*, Springer Science & Business Media, 2013.

[22] R. W. Stewart, K. W. Barlee, D. S. Atkinson, and L. H. Crockett, *Software Defined Radio Using MATLAB & Simulink and the RTL-SDR*, Strathclyde Academic Media, 2015.

[23] M. Rice, *Digital communications: A Discrete-time Approach*, Pearson Education India, 2009.

[24] H. Meyr, M. Moeneclaey, and S. A. Fechtel, *Digital Communication Receivers: Synchronization, Channel Estimation, and Signal Processing*, Wiley Online Library, 1998.

Mir Lodro is a Ph.D. student at George Green Institute for Electromagnetics Research-GGIEMR, University of Nottingham, UK. He has received a Master of Research-MRes in Electrical and Electronic Engineering from the same university in 2015. His areas of research interests are SDR based prototype development for channel measurements and modeling, wireless digital receiver design, reverberation chamber based measurements, channel modeling for short-range wireless communication such as wireless chip-to-chip communication, MIMO measurements, Large Intelligent Surface (LIS), 5G/6G wireless communication.

Chris Smart has received his MEng. and Ph.D. degrees in Electrical and Electronic Engineering from the University of Nottingham in 1991 ans 1995 respectively. Following two years working as a Research Assistant at the University of Nottingham, he joined BAE SYSTEMS where he worked on 2D and 3D full field time domain techniques for electromagnetic field simulation for aerospace applications. In 2007 he re-joined the George Green Institute for Electromagnetics Research at the University of Nottingham as a Research Fellow where his research interests include the development and application of computational electromagnetics methods and the development techniques for time domain measurement of electromagnetic field including near-field methods, with applications to EMC and EMI studies.

Gabriele Gradoni received the Ph.D. degree in electromagnetics from the Università Politecnica Delle Marche, Ancona, Italy, in 2010. In 2008, he was a Visiting Researcher with the Time, Quantum Electromagnetics Team, National Physical Laboratory, Teddington, U.K. From 2010 to 2013, he was a Research Associate with the Institute for Research in Electronics and Applied Physics,University of Maryland, College Park, MD, USA.From 2013 to 2016, he was a Research Fellow with the School of Mathematical Sciences, University of Nottingham, U.K. Since 2016, he has been an Associate Professor of mathematics and electrical engineering with the University of Nottingham. His research activity is in probabilistic and asymptotics methods for propagation in complex wave systems, wave chaos, and MIMO wireless systems. He is a member of the American Physical Society and the Italian Electromagnetics Society. He was a recipient of the URSI Commission B Young Scientist Award in 2010 and 2016, and the Gaetano Latmiral Prize in 2015. Since 2014, he has been the URSI Commission E Early Career Representative.

Ana Vukovic was born in Nis, Serbia, in 1968. She received the Diploma of Engineering degree in electronics and telecommunications from the University of Nis, Nis, Yugoslavia, in 1992 and the Ph.D. degree from the University of Nottingham, UK in 2000. From 1992 to 2001, she was a Research Associate with the University of Nottingham. In 2001, she joined the School of Electrical and Electronic Engineering, University of Nottingham, as a Lecturer. Her research interests are electromagnetics with a particular emphasis on applications in optoelectronics, microwaves and EMC.

Dave Thomas is a Professor of Electromagnetics Apllications and Director of The George Green Institute for Electromagnetics Research, The University of Nottingham, UK. His research interests are in electromagnetics compatibility, electromagnetics simulation, power system transients and power system protection. He is member of CIGRE and convenor for Joint Working Group C4.31 “EMC between communication circuits and power systems”, Chair of COST Action IC 1407 “Advanced Characterisation and Classification of Radiated Emissions in Densely Integrated Techniques (AcCREDIT)” and member of the EMC Europe International Steering Committee.

Steve Greedy was born in Cardiff, UK. He received the MEng. and Ph.D. degrees in 1998 and 2002 from the University of Nottingham. He is an Associate Professor within George Green Institute for Electromagnetics Research. His interests are in the area of experimental and computational electromagnetics with a focus on techniques used in the study of electromagnetics compatibility and signal integrity, specifically mechanisms that impact performance of wired and wireless communication systems.